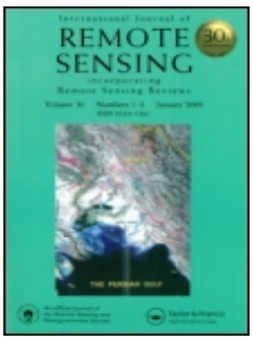

International Journal of Remote Sensing

ISSN: 0143-1161 (Print) 1366-5901 (Online) Journal homepage: https://www.tandfonline.com/loi/tres20

# A coupled Land Atmosphere Radiative-Transfer Model (LA-RTM) for multi-frequency passive microwave remote sensing: development and application over Wakasa Bay and the Tibetan Plateau

David Kuria , Toshio Koike , Hui Lu , Tobias Graf & Hiroyuki Tsutsui

**To cite this article:** David Kuria , Toshio Koike , Hui Lu , Tobias Graf & Hiroyuki Tsutsui (2011) A coupled Land Atmosphere Radiative-Transfer Model (LA-RTM) for multi-frequency passive microwave remote sensing: development and application over Wakasa Bay and the Tibetan Plateau, International Journal of Remote Sensing, 32:6, 1779-1796, DOI: 10.1080/01431161003621627

**To link to this article:** https://doi.org/10.1080/01431161003621627

*International Journal of Remote Sensing*
Vol. 32, No. 6, 20 March 2011, 1779–1796

Taylor & Francis
Taylor & Francis Group

# A coupled Land Atmosphere Radiative-Transfer Model (LA-RTM) for multi-frequency passive microwave remote sensing: development and application over Wakasa Bay and the Tibetan Plateau

DAVID KURIA*†, TOSHIO KOIKE‡, HUI LU‡, TOBIAS GRAF‡ and HIROYUKI TSUTSUI‡

†Department of Geomatic Engineering and Geospatial Information Systems, Jomo Kenyatta University of Agriculture and Technology P.O. Box 62000-00200, Nairobi, Kenya

‡Department of Civil Engineering, River and Environmental Engineering Laboratory, University of Tokyo, Tokyo 113-8656, Japan

(*Received 29 December 2008; in final form 8 January 2010*)

Multi-frequency passive microwave sensors herald a new dawn for combined land and atmosphere observations. Past efforts to utilize microwave remote sensing of atmosphere and land surface have proceeded by treating these two areas in a parallel fashion. In this research, a unified approach is presented that can be used to improve both quantitative and qualitative understanding of land and atmosphere constituents. A coupled Land Atmosphere Radiative-Transfer Model (LA-RTM) that can be used as a forward model in retrieval algorithms, or as an observation operator in data-assimilation schemes is developed. This model is validated using data collected during the 2003 Advanced Microwave Scanning Radiometer on board the Earth Observing Satellite (AMSR/AMSR-E) validation experiment over Wakasa Bay in Japan and the Coordinated Enhanced Observing Period (CEOP) dataset for the Tibetan Plateau collected in April and August 2004. These datasets comprise satellite (AMSR-R) observations, ground-based microwave radiometers (GBMRs) and radiosonde atmosphere soundings. In both sites, good agreement between simulated and observed brightness temperatures is demonstrated. To facilitate fast retrievals, a retrieval scheme is proposed that uses LA-RTM as a forward model to generate a look-up table (LUT) for varying land-surface conditions. This LUT is used to retrieve soil-moisture and surface-roughness conditions for the target site. Using this scheme, retrieved soil moisture at *in situ* stations was shown to have fairly good agreement with observations.

## 1. Introduction

In the recent past, much progress has been made in passive microwave remote sensing of land (Ulaby *et al.* 1986, Njoku 1999) and atmosphere (Wilheit *et al.* 1999, Kummerow *et al.* 2001). Much of this work has, however, been carried out in a somewhat parallel fashion. In passive microwave remote sensing of land-surface conditions, typically LX microwave bands are used, due to their ability to penetrate cloud and light precipitation (Ulaby *et al.* 1981). Higher microwave frequencies (>20 GHz) contain information about atmosphere, but, over land, it is difficult to

*Corresponding author. Email: dn.kuria@gmail.com

*International Journal of Remote Sensing*
ISSN 0143-1161 print/ISSN 1366-5901 online 
http://www.tandf.co.uk/journals
DOI: 10.1080/01431161003621627

obtain this information as the land surface gives very large and heterogeneous emissions in comparison to that contributed by the atmosphere. In contrast, the sea surface at microwave frequencies is imaged as a cold and nearly homogeneous target, and thus atmosphere information can be obtained with a reasonably higher degree of confidence. Hence, most atmosphere research with microwaves has tended to be over oceans (Kummerow *et al.* 2001, Shin and Kummerow 2003).

To obtain atmosphere information over land using passive microwaves, it is essential to estimate surface emission reasonably well, thereby addressing the heterogeneity problem. Kuria *et al.* (2007) demonstrated that by inclusion of shadowing in the Advanced Integral Equation Model (AIEM), it is possible to obtain bare wet surface emission with a high degree of confidence. In their experiment-supported work, they showed that AIEM simulations agreed well with observations, if shadowing was included. Because they dealt with bare wet surfaces, volume-scattering effects were negligible and were therefore ignored. Lu (2006) showed that in the case of very dry soil, volume scattering should be considered. It was shown that a coupling of Dense Media Radiative Transfer (DMRT) developed by West *et al.* (1993) with a modified four-stream model for soil developed by Fujii and Koike (2001) represents volume scattering in a physically consistent manner.

Liu (1998) developed a four-stream radiative-transfer model (RTM) for plane parallel and horizontally homogeneous atmospheres. He showed that four-stream approximation accuracy does not degrade significantly in comparison to an accurate 32-stream model while registering huge computational time savings.

Fujii and Koike (2001) developed a rainfall retrieval algorithm using the Tropical Rainfall Monitoring Mission (TRMM) Microwave Imager (TMI) dataset. In their scheme, they used 10.65 and 85 GHz vertically polarized data to retrieve corresponding rain signatures, which they related to observed radar data. They obtained some level of agreement with observations rainfall, but their model assumed vegetation and roughness effects, and ignored the effects of other hydrometeors.

Much work has therefore been carried out by various researchers. This article seeks to combine these efforts to improve the definition of surface emission and radiative transfer in the soil and atmosphere by coupling these various models, both for modelling land-surface emissions and atmospheric emissions.

Formally, the objectives of this article are to: (i) develop a coupled Land Atmosphere Radiative-Transfer Model (LA-RTM), (ii) evaluate the performance of this RTM, (iii) develop a land-surface variable retrieval algorithm and (iv) retrieve the prevailing land-surface condition.

## 2. Model description

As microwave radiations propagate further through the atmosphere while emanating from the land surface and atmosphere, they encounter scattering, absorption and re-emission that are dependent on the properties of the media and particles they encounter. All these various scattering, emission and absorption processes are occurring simultaneously, and thus there is need to develop an encompassing and physically based model that couples individual models used to study each individual process. Such a model has been developed in this article to address radiative transfer on land and in atmosphere.

Figure 1 shows the various sub-models that comprise the proposed model. Also shown are the processes that each of the sub-models predominantly account for. This model is referred to as the LA-RTM. Over oceans, seas and other water bodies,

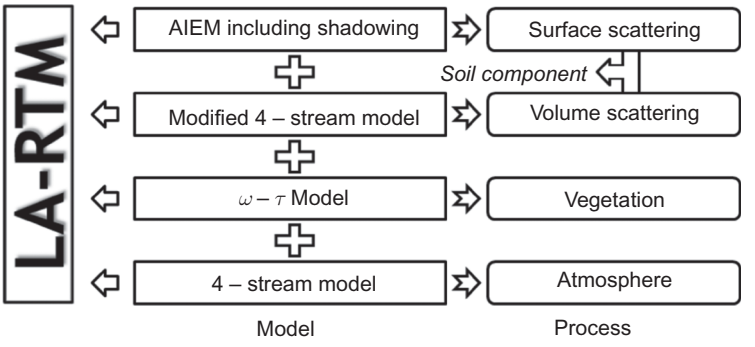


Figure 1. Sub-models that comprise the proposed model (LA-RTM) and the predominant processes that each of them models.

LA-RTM uses the four-stream model developed by Liu (1998) for modelling radiative transfer in the atmosphere. A land ocean flag is used to decide how to consider surface emission, that is, over ocean or over land. Over land, LA-RTM treats volume scattering within the soil volume through a modified four-stream model for soil developed by Lu (2006). This modified four-stream model uses DMRT theory (West *et al.* 1993) to calculate the extinction coefficient $\kappa_e$ and effective propagation constant. Surface scattering is treated using a modified AIEM that includes shadowing effects of rough surfaces, as validated by Kuria *et al.* (2007). The dielectric constant for soil required by LA-RTM is computed according to Dobson *et al.* (1985) including further enhancements by Peplinski *et al.* (1995). Over vegetated terrain, scattering and emission are accounted for by the $\omega - \tau$ model (Jackson and Schmugge 1991, Schmugge and Jackson 1992). Atmospheric scattering and emission are handled using the four-stream model developed by Liu (1998), and improved upon by Pfaff (2003). Modelling of scattering and absorption in the atmosphere is very dependent on the type of particle-size-distribution functions adopted. In this model, rainfall scattering and absorption calculations are carried out using the Marshall–Palmer distribution (Marshall and Palmer 1948), while snowfall is treated using an exponential distribution function developed by Sekhon and Srivastava (1970). Cloud-droplet water effects are calculated using Mie's theory. The particle-size-distribution function for cloud ice resembles that of cloud liquid water (Pfaff 2003).

Table 1 shows the various options available in the use of LA-RTM. These options are given depending on surface type, surface conditions and target application.

For a wet, rough, bare surface under clear-sky conditions utilizing lower microwave frequencies, option 1 will ensure faster processing without significant deviation from the result obtained using all the sub-models. Option 2 is for the case of a wet rough surface overlain by a layer of vegetation using lower frequencies. Option 3 can be used under similar conditions as for option 2, but in this case, the effects of atmosphere are significant (such as when using higher microwave frequencies). Option 4 considers the situation similar to that for option 1, but for higher microwave frequencies. Options 5–8 follow similar arguments, but in all the cases, the soil layer is not very wet and thus the effects of volume scattering within the soil layer are not negligible. Option 9 considers the situation where instead of the land surface, the surface is water. In this case, to obtain surface emission, the required variables are sea-surface wind speed, sea-surface temperature and the salinity.

Table 1. Various options available when using LA-RTM.

| Option | Sub-models involved |
|---|---|
| 1 | AIEM only |
| 2 | AIEM + Vegetation |
| 3 | AIEM + Vegetation + Atmosphere |
| 4 | AIEM + Atmosphere |
| 5 | Soil RTM only |
| 6 | Soil RTM + Vegetation |
| 7 | Soil RTM + Vegetation + Atmosphere |
| 8 | Soil RTM + Atmosphere |
| 9 | Water surface + Atmosphere |

Note: Soil RTM refers to a coupling of four-stream for soil incorporating DMRT (volume scattering) with AIEM (surface scattering) Water surface refers to lower boundary being water and not land.

The required inputs for LA-RTM are listed in table 2. These are divided into five broad categories, namely, (i) common, (ii) ocean, (iii) soil, (iv) vegetation and (v) atmosphere. Details for the expected variables under each category are given in this table.

## 3. Study areas

Data to validate the proposed model were collected from two sites during two different time periods. In 2003, intensive ground-based and satellite observations were conducted in Wakasa Bay, Japan. In 2004, several ground-based measurements of soil-moisture and atmosphere soundings were conducted over the Tibet Coordinated Enhanced Observing Period (CEOP) project site, China.

### 3.1 *Wakasa Bay site*

To obtain a dataset comprising radiometer data and information about the state of the atmosphere, observations were carried out as part of the Advanced Microwave Scanning Radiometer on board the Earth Observing Satellite (AMSR/AMSR-E) validation program at Wakasa Bay (Pfaff 2003). Wakasa Bay is located near Fukui City, Fukui Prefecture, Japan at about 36° N and 136° E. Measurements included rawinsonde observations, observations by research vessels located in the Japanese Sea, radar observations and various ground observations ranging from standard meteorological data, such as air temperature, wind speed and direction, to ceilometer and radiometer measurements, as well as sophisticated particle-size observation systems. The site had been set up using the facilities of Fukui airport. This site was selected due to the relative homogeneity of surrounding areas, and an unobstructed line of sight in the case of radar observations.

To obtain atmospheric pressure, temperature, humidity profiles, wind speed and direction, radiosondes were launched four times a day at 00:00 Coordinated Universal Time (UTC), 05:00 UTC, 12:00 UTC and 18:00 UTC during the intensive observation periods and at 00:00 UTC, 05:00 UTC and 12:00 UTC during the routine observation periods. The launch at 05:00 UTC was taken in deviation from the usual World Meteorological Organizations (WMOs) procedures, so as to guarantee a measurement of atmospheric profile, nearly coincident with the AMSR-E overpass time.

Table 2. Required information to run LA-RTM.

| Part | Variable | Description |
|---|---|---|
| Common | FR | Operating frequency (GHz) |
| | THETA | Incidence angle |
| | IPOL | Polarization to consider (1 or both) |
| | OLF | Ocean or land flag (0 [ocean] or 1 [land]) |
| Ocean | SAL | Salinity (ppm) |
| | SST | Sea-surface temperature (K) |
| | SSW | Sea-surface wind speed (m $s^{-1}$) |
| Soil | LL | Number of soil layers |
| | TS | Soil temperature for each soil layer (K) |
| | MV | Soil moisture for each soil layer ($m^3$ $m^{-3}$) |
| | RHOB | Soil bulk density in each layer (g $cm^{-3}$) |
| | RHOSS | Soil solid density in each layer (g $cm^{-3}$) |
| | SA | Sand fraction in each layer |
| | CL | Clay fraction in each layer |
| | SIG | Root mean square (r.m.s.) height of surface layer (cm) |
| | CORL | Correlation length of surface layer (cm) |
| | *P* | Parameter in Gaussian distribution for DMRT |
| | *Q* | Parameter in Gaussian distribution for DMRT |
| | NA | Number of distinct particle sizes ($= 1$ or $> 5$) |
| | ZS | Soil-depth profile (m) |
| | FTOT | Total soil fraction including soil moisture |
| | RD | Mode radius of soil particles (cm) |
| | RBG | Flag to use rough background surface or smooth one |
| Vegetation | B1 | Vegetation parameter |
| | WE | Vegetation water content |
| | OM | Vegetation single-scattering albedo |
| | *X* | Vegetation parameter |
| | TC | Temperature at top of vegetation canopy (K) |
| Atmosphere | *L* | Number of atmosphere layers |
| | *Z* | Height profile (m) |
| | TK | Air-temperature profile (K) |
| | PMB | Air-pressure profile (mb) |
| | RH | Relative humidity (%) |
| | RR | Rain-rate profile (mm $hr^{-1}$) |
| | CW | Cloud liquid-water content (g $m^{-3}$) |
| | CI | Cloud ice content (g $m^{-3}$) |
| | SR | Snowfall-rate profile (mm $hr^{-1}$) |
| | DOPT | Option to use four-stream approximation or DOM approach |

During the experimental period, three ground-based microwave radiometers (GBMRs) were used. These were a Radiometrics WVR-1100 two channel radiometer and two newly developed radiometers designated RPG-LWP and RPG-TEMPRO 90 (RPG Radiometer Physics Gmbh, Meckenheim, Germany). The WVR-1100 is an unpolarized radiometer observing the sky at 23.8 and 31.4 GHz. Its accuracy is given by the vendor to be 0.3 K with a resolution of 0.25 K and one measurement approximately every 40 s. This is a widely used system and it was used to provide a comparison to the new radiometers.

The RPG-LWP is similar to the WVR-1100 as it measures brightness temperatures at 23.8 and 36.5 GHz. It is a non-polarized sky radiometer with a resolution of 0.2 K for an integration time of 1 s and an overall system stability of 1 K. This radiometer was connected to the RPG-TEMPRO 90 so that both instruments could provide

time-synchronized data. The RPG-TEMPRO 90 is a radiometer designed to retrieve temperature profiles of the atmosphere by scanning the left flank of the oxygen line at 60 GHz as well as to improve water vapour and cloud liquid-water measurements. It operates at nine frequencies ranging from 50.8 to 58.8 GHz and has an additional 90.0 GHz channel for use with the two RPG-LWP channels to improve water-vapour and liquid-water path retrievals. The nine profiling channels had a time resolution of approximately 20 s, which corresponds to an integration time of roughly 2 s per channel, while the 90 GHz channel was operated similarly to the LWP channels at 1 s integration time (Rose and Zimmermann 2003). All radiometers were operated at a viewing angle of 35.0° elevation from inside a garage, where they were protected from rain and snowfall. The elevation angle coincides with the observation angle of 55° from nadir of the AMSR and AMSR-E instruments. AMSR-E brightness-temperature imagery was provided for the validation exercise.

### 3.2 *Tibet CEOP site*

Figure 2 shows part of the Tibet CEOP site including four *in situ* stations. The CEOP project was initiated to bring together research activities in the Global Energy and Water Cycle Experiment (GEWEX) and related activities of the World Climate Research Program (WCRP). The CEOP project has developed a comprehensive network of *in situ* stations distributed around the world, and among them is the

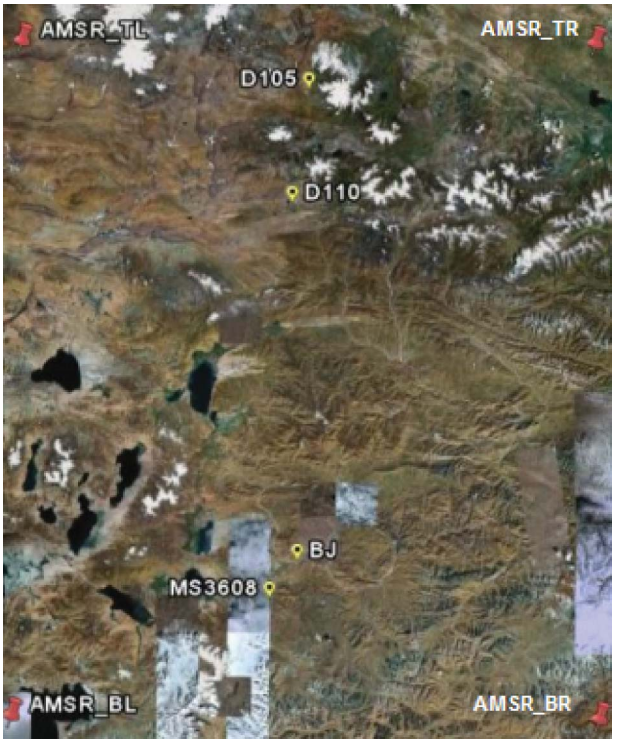


Figure 2. The CEOP Tibet site. The red pegs mark the extents corresponding to AMSR-E image. Four *in situ* stations are marked with small yellow pegs. This image was obtained from Google Earth™ and covers the region 29° N–34° N and 89° E–94° E (490 km × 540 km). © 2008 Google: Mapdata © 2008 Mapabc, Image © 2008 GeoEye, Image © 2008 Terrametrics.

Tibet CEOP site. The Tibetan Plateau is 4000 m above sea level, 3000 km long in longitude and 1000 km wide in latitude. It experiences strong surface solar radiation, has low pressure, low air density, but a wide range of air temperatures. It experiences strong diurnal and seasonal variation of land cover, energy partition, cloud cover and rainfall. During the monsoon season, it experiences a lot of rainfall, but there is a big contrast in rainfall and land cover between eastern and western parts of the plateau (Yang *et al.* 2005). The plateau surfaces are typically characterized by alpine meadows and grasslands in the central and eastern parts, while the western part is dominated by alpine deserts (Yang *et al.* 2009).

The match-up dataset consists of brightness-temperature data observed by the AMSR-E and *in situ* data measured by the Soil Moisture and Temperature Measuring System (SMTMS) and Automatic Weather Station (AWS) from January to December 2004. The coverage of AMSR-E image dataset is $2.5^\circ \times 2.5^\circ$, with a sampling resolution $0.05^\circ$ for all frequencies. The *in situ* data consists of soil-moisture and soil-temperature data, observed at 0.03 and 0.10 m depths. The dataset is provided as a brightness-temperature raster image for whole area, and a text file for each of the CEOP stations.

The text files record AMSR-E brightness-temperature and *in situ* data at each station. The *in situ* data includes observations 12 hours prior to, and 12 hours after, the AMSR-E overpass. In this research, match-up *in situ* data at AMSR-E overpass time are calculated by linearly interpolating to the minute, the *in situ* data on the hour prior to, and the hour after, overpass. In this research, data from stations BJ and D110 were used. The geographic location details are $31.37^\circ$ N, $91.90^\circ$ E, with an elevation of 4509.20 m.

During the months of April and August 2004, regular rawinsonde launches were made in Tibet. For this period, AMSR-E imagery was available. However, information about observed precipitation for the site was lacking. To mitigate this lack, the Advanced Regional Prediction System (ARPS), a terrain following non-hydrostatic model developed by Xue *et al.* (2003), was used to generate atmospheric condition information. The initial conditions and boundary conditions were provided by the National Centers for Environmental Prediction (NCEP) Global Forecast System (GFS) Global Circulation Model (GCM) reanalysis data. Data for this site were obtained utilizing the CEOP Client, a tool for interrogating, subsetting and downloading data available at CEOP sites. This tool was developed by Nemoto *et al.* (2007).

## 4. LA-RTM model validation

Both the Wakasa 2003 experiment and the CEOP Tibet site datasets were used to validate LA-RTM. The Wakasa dataset was used to validate the model's performance over water bodies, while the Tibet dataset was used to validate the model's performance over land.

### 4.1 *Application of LA-RTM over Wakasa Bay*

To assess the validity of the model in the absence of observed detailed hydrometeor profiles, cloud-free datasets were used. In this experiment, there were no measurements of soil properties and land-surface conditions during the GBMR experiment, and thus, model performance over land at this site could not be undertaken using this

dataset. Its performance assessment was therefore restricted to its capacity to capture the propagation of microwave radiation over the Pacific Ocean.

To run the model for satellite-simulated observations, one needs to specify the boundary condition, that is, either land surface or ocean surface. In this case, the boundary condition is ocean surface, and information about sea-surface wind speeds, sea-surface temperatures and salinity of the sea water are required. An AMSR-E image grid point located in the Pacific Ocean at 33° N, 136° E, which is close to the coastline allows one to assume that the sonde profile launched from the bay during GBMR observation can be assumed to represent it too, but is far enough away from the coastline to ensure that the selected grid does not have contamination from the land surface.

To identify the cloud-free dataset, the Atmospheric Infrared Sounder (AIRS) cloud-top temperature product (figure 3(*a*)), in conjunction with the Geostationary Meteorological Satellite (GMS) cloud-coverage image (figure 3(*b*)), was used. To obtain sea-surface variables, the Moderate Resolution Imaging Spectroradiometer (MODIS) sea-surface temperature product (figure 3(*c*)) and MODIS sea-surface wind speed (figure 3(*d*)) were used. To provide the requisite temperature profile, pressure profile and relative humidity (RH) profile, sonde observations (figure 3(*e*)) were used.

AMSR-E brightness-temperature images for the whole duration of the field observations were acquired. Satellite brightness temperatures for the selected grid were subsequently obtained from these images. Comparisons of these observed satellite brightness temperatures with simulated ones over the ocean surface were conducted. Satellite image grids over land were not considered because, as mentioned earlier, observations of land-surface conditions were not undertaken, and hence the restriction to consider only the ocean cases.

Figure 4 shows the comparison between observations and simulations for selected cloud-free days. Figure 4(*a*) shows a comparison for 24 January 2003. From the scatterplot presented in the inset, the coefficient of determination is $R^2 = 0.697$, signifying a very good correspondence. It can be noted that generally, at all frequencies, there is agreement between simulations and observations. At frequencies lower than 23 GHz, there is perfect correspondence between simulation and observations. To show the performance of the model for several days, a comparison of scatterplots for 2 days is given (figure 4(*b*)). In this case, there is a linear relationship, with $R^2 = 0.996$, signifying very good correspondence. This therefore confirms that LA-RTM is valid for clear-sky conditions over sea or ocean surfaces.

Subsequently, a comparison of LA-RTM's performance in simulating GBMR observations is considered. In this case, days that were observed to be cloud free during GBMR observations were considered. The 'hot and cold' load calibration method was used to calibrate these radiometers. The observed brightness temperatures showed agreement with simulations from LA-RTM. Sonde observations were used to provide temperature, pressure and RH profiles needed by the RTM model.

Figure 5 shows a comparison of observations and simulation for 13 January 2003. In the inset, a linear relationship between observations and simulations is given. It can be noted that the maximum discrepancy is 3 K, which is quite good. The coefficient of determination is $R^2 = 0.994$, which implies that there is very good correspondence.

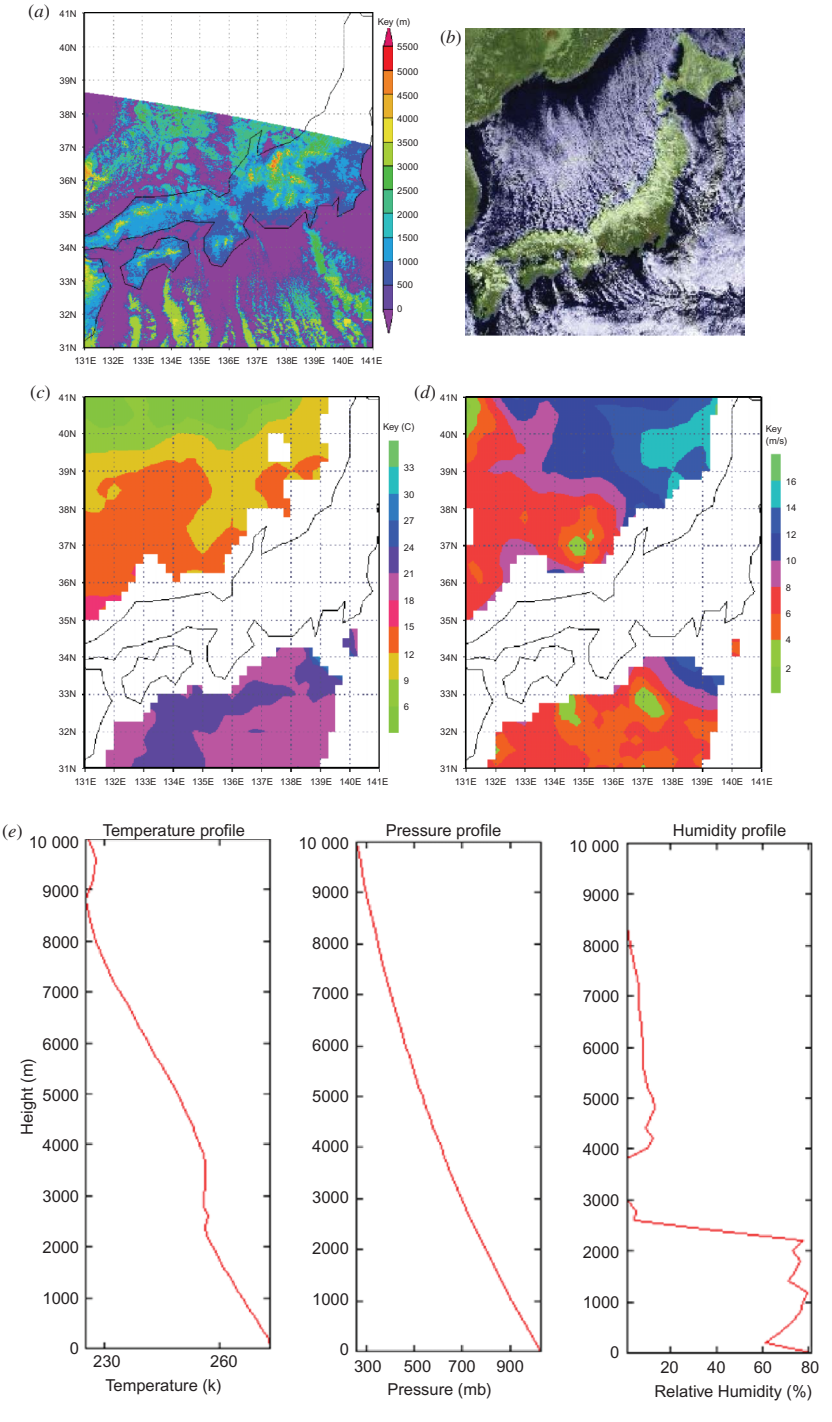


Figure 3. Dataset used to run four-stream model over the Pacific Ocean (*a*) Atmospheric Infra Red Sounder (AIRS) cloud-top elevations (m), (*b*) Geostationary Meteorological Satellite (GMS) cloud-cover image, (*c*) Moderate resolution Imaging Spectroradiometer (MODIS) sea-surface temperature (°C), (*d*) MODIS sea-surface wind speed (m $s^{-1}$) and (*e*) sonde profiles.

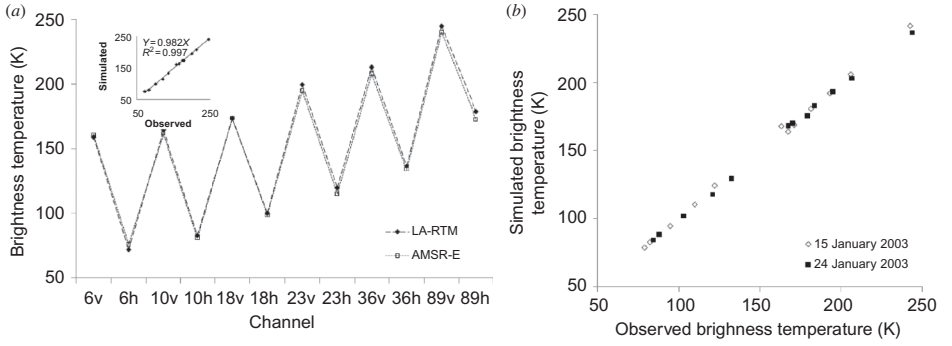


Figure 4. Relationship between satellite observations viz. simulations for Wakasa Bay: (*a*) comparison for 24 January 2003. The inset shows the scatterplot of simulated brightness temperatues (LA-RTM) against observed brightness temperatures (AMSR-E) in K. (*b*) Comparison for 2 days.

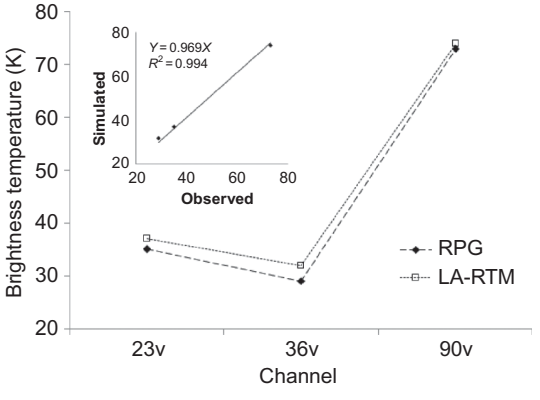


Figure 5. Comparison of GBMR observations against simulations. Inset: corresponding scatterplot for the brightness-temperature (K) simulations (LA-RTM) against observations (RPG).

### 4.2 *LA-RTM validation and verification over CEOP Tibet*

Before proceeding with LA-RTM validation over land, a comparison of atmospheric profiles observed during sonde launches with simulations from the mesoscale model was conducted.

Figure 6 shows some of the profiles obtained from the ARPS compared with sonde observations. To obtain potential temperature, $\theta$, the potential-temperature formulation $\theta = T\left(\frac{P_0}{P}\right)^{0.286}$ was used, where $T$ is air temperature, $P_0$ is reference pressure (mean sea-level pressure) and $P$ is air pressure. There is good correspondence between potential-temperature profiles (figure 6(*b*)). It can be noted that overall, the potential-temperature profiles agree fairly well at all elevations. Comparing the RH profiles (figure 6(*a*)), it can be noted that, overall, the mesoscale model is again able to simulate the RH profile reasonably well. At the lower altitudes, which contain most of the water vapour in the column, the observed RH profiles show fairer agreement with simulation.

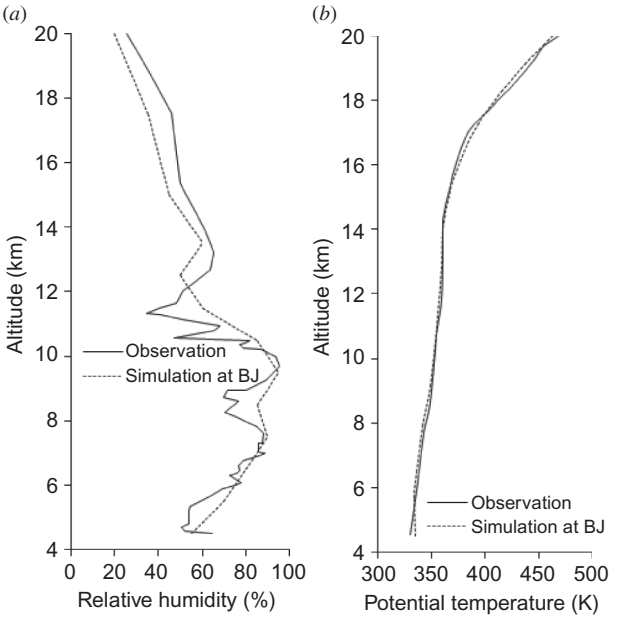


Figure 6. Comparison of ARPS simulated (simulation at BJ) relative humidity and potential-temperature profiles with observation (sounding) at BJ CEOP Tibet site.

From these simulation results, it can be concluded that the ARPS atmospheric water-vapour product can be used in situations where observed atmospheric sounding data may not be available, or its quality may be suspect. Since no observed precipitation or cloud information was available, it was thus assumed that the product from the mesoscale model could be used as the input for LA-RTM.

Evaluation tests were conducted to assess the performance of the developed LA-RTM using sonde profiles augmented by model profiles where sonde profiles were not taken. For this evaluation, the BJ site simulation data were considered since sonde launches were done close to this site (within ~2 km). Soil moisture and temperature measurement system (SMTMS) observations for obtaining soil-moisture and temperature profiles, sonde or ARPS simulations for air temperature, air pressure and RH profiles were used. Vegetation parameters were estimated using satellite data according to Sellers *et al.* (1996), with precipitation and cloud information coming from the mesoscale model (ARPS simulations).

In figure 7, a comparison of LA-RTM simulation, surface emission only simulation and observations for 14 August at AMSR-E overpass time is shown. The surface-emission model (AIEM), in this case, considers shadowing effects, but ignores atmosphere effects. Using ARPS output, it is noted that LA-RTM is able to consider the effects of the atmosphere in a consistent fashion, giving better agreement with observations at all frequencies than the AIEM. This is better visualized when the inset scatterplot is inspected. It can be seen that LA-RTM gives a better linear fit than the surface-emission model. Errors in depicting atmosphere conditions are shown to make the surface-emission simulation at higher frequencies deviate from observations since it ignores attenuation by atmospheric constituents. The AIEM is able to simulate lower frequency observations well, but due to it ignoring atmosphere conditions, it is not able to simulate higher frequencies as well. At lower

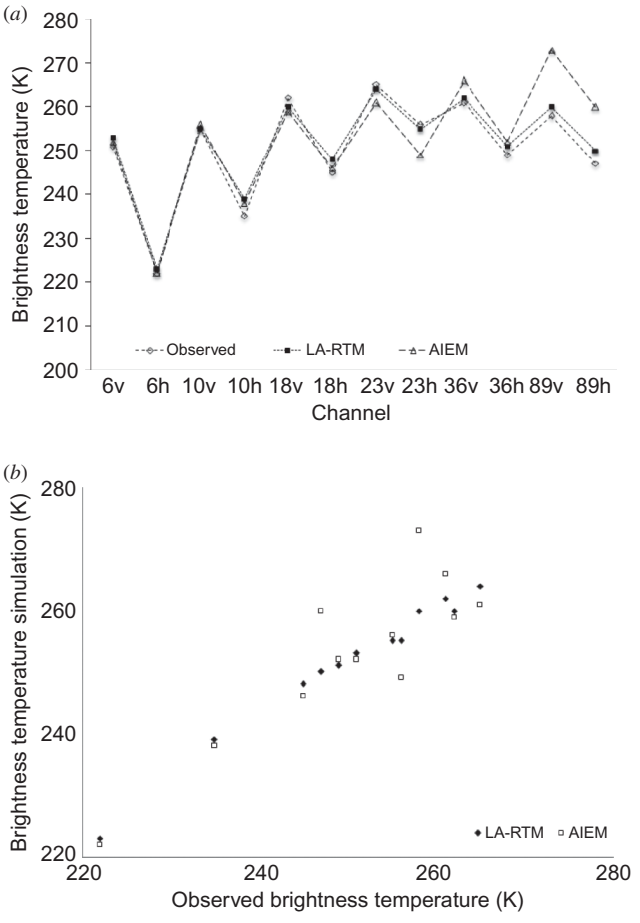


Figure 7. (*a*) Performance of LA-RTM against the AIEM (includes shadowing) and corresponding satellite brightness temperatures. (*b*) Scatterplots of both LA-RTM against satellite brightness temperatures and the AIEM against satellite brightness temperatures.

frequencies (6.925–18.7 GHz), the AIEM and LA-RTM agree, as expected since, at these frequencies, the atmosphere is transparent to microwaves.

## 5. LA-RTM forward modelling as an aid to retrieval of surface variables

LA-RTM is a coupling of theoretical models that represent various processes as radiation interacts with particles and media. These processes are complex and, as a consequence, the model is substantially complex; for operational applications, this can be a limiting factor due to intense computational demands. It was found desirable therefore to investigate its use in development of a retrieval scheme for surface variables, which uses its physical basis but does not require the same computational resources.

### 5.1 *Land-surface variables retrieval scheme*

A retrieval scheme for soil moisture is proposed that makes use of the polarization index (PI) (Paloscia and Pampaloni 1988) using 6.925 GHz, and an index of soil

wetness (ISW) (Fujii and Koike 2001) using horizontally polarized brightness-temperature difference for 6.925 and 18.7 GHz. Look-up tables (LUTs) were prepared by running LA-RTM as a forward model under varying moisture and roughness conditions. It is assumed that moisture and roughness have the largest impact on emissivity than other parameters at lower frequencies. The PI and ISW were computed using the two equations

$$\mathrm{PI}_6 = \frac{T_{\mathrm{B}_{6\mathrm{v}}} - T_{\mathrm{B}_{6\mathrm{h}}}}{\frac{1}{2}(T_{\mathrm{B}_{6\mathrm{v}}} + T_{\mathrm{B}_{6\mathrm{h}}})}, \tag{1}$$

$$\mathrm{ISW} = \frac{T_{\mathrm{B}_{18\mathrm{h}}} - T_{\mathrm{B}_{6\mathrm{h}}}}{\frac{1}{2}(T_{\mathrm{B}_{18\mathrm{h}}} + T_{\mathrm{B}_{6\mathrm{h}}})}, \tag{2}$$

where $\mathrm{PI}_6$ refers to the polarization index obtained using brightness-temperature values ($T_\mathrm{B}$) obtained from the horizontally polarized (h) emissions and vertically polarized (v) emissions at 6.925 GHz. The subscripts (6 and 18) are simplifications referring to the 6.925 and 18.7 GHz frequencies. The PI can be obtained for any frequency at which both vertically and horizontally polarized brightness-temperature observations are available.

To generate the LUT, the following specifications were adopted: one soil layer; soil temperature = 283 K; sand fraction = 0.6; clay fraction = 0.2; soil bulk density = 1.258; mode radius = 0.08 cm; incidence angle = 55°; layer depth = 5 cm; $P = 2$; $Q = 10$; number of distinct particles sizes = 1, where $P$ and $Q$ are parameters in the Gaussian distribution function used in Dense Media Radiative Transfer (DMRT). These were found representative of the target area of application. An idealized clear-sky atmosphere (International Standard Atmosphere) was used. Surface-roughness conditions were retrieved by assuming that over time, they are invariant. Koike *et al.* (1996) derived linear relationships between root mean square (r.m.s.) heights and correlation lengths for the Tibetan Plateau. They showed that these approximations were valid for applications retrieving soil-wetness information from satellite data. They assumed that surface-roughness conditions were invariant for the duration of about 1 month. In this research, retrieved surface-roughness conditions at four stations in Tibet (BJ, D105, D110 and MS3608) were used to develop the following relationship, which can be used to relate correlation length to retrieved r.m.s. height for any grid point at the Tibet site

$$l = 2.5\sigma - 0.21, \tag{3}$$

where $l$ is correlation length and $\sigma$ is r.m.s. height. The forward model was run by varying the r.m.s. height from 0.30 to 1.30 cm at intervals of 0.01 cm, and moisture conditions from 0.1% to 50%. A random dataset within these specifications was also generated.

Figure 8 shows these randomly generated data superimposed on part of the LUT. It can be seen from the distribution of the randomly generated points that it is possible to retrieve soil-moisture and surface-roughness conditions for most of the points using this LUT. From this result, it can therefore be hypothesized that it is possible to use this LUT scheme to retrieve soil-moisture and surface-roughness conditions for the Tibet site where the roughness condition is defined as $\theta = \frac{\sigma}{l}$. Using equation 3, $\sigma$ and $l$ can be obtained.

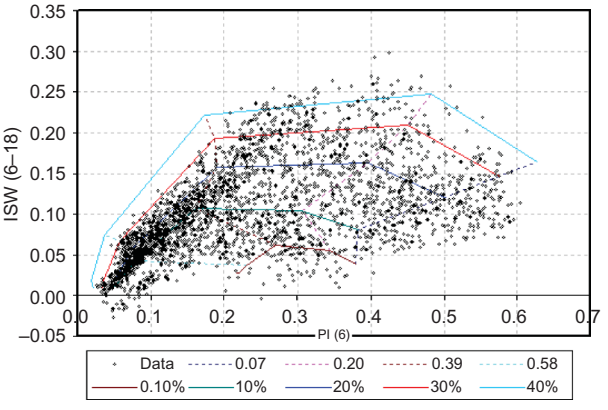


Figure 8. PI–ISW look-up table. Solid lines represent roughness conditions and dashed lines represent soil-moisture conditions. PI was derived using 6.925 GHz (abbreviated as 6 in the figure), while ISW was derived using a combination of 6.925 GHz and 18.7 GHz (abbreviated as 6–18 in the figure).

### 5.2 In situ *retrieval results*

The LUT generated above was applied to satellite data for the CEOP Tibet station BJ. The satellite data used in calculating the retrievals was resampled to 0.05° (~5 km). Yang *et al.* (2007) demonstrated that, using AMSR-E data resampled to 0.1°, it was possible to obtain representative soil-moisture distribution in the Tibetan Plateau agreeing with *in situ* observations. In this research a finer resolution (0.05°) is considered. The considered *in situ* stations are (for BJ) in the valley region and (for D110) in elevated parts where there was considerable thawing during the observation period. It is assumed in this research that the soil-moisture conditions in these regions are nearly homogenous (Yang *et al.* 2005).

The soil-moisture retrieval steps are to (i) calculate PI and ISW using observed brightness temperatures and (ii) use the calculated PI and ISW to look up the corresponding moisture (Mv) and roughness parameter. As assumed earlier, the roughness parameter is constant for the site, with the r.m.s. height being 0.48 cm and the correlation length being 0.96 cm. These values were arrived at by obtaining the average retrieved roughness conditions for the site from time-series satellite data for the month of August 2004. Figure 9 shows the results of soil-moisture retrieval using the PI–ISW LUT.

Both AMSR-E ascending and descending passes were considered in the preparation of data for comparison purposes. The retrieval results show reasonable retrieval capabilities of this algorithm. Maximum differences between observations and simulations are ~5%, which could be due to active precipitation during overpass times, or due to the error introduced by comparing grid-scale soil moisture (aggregated over 5 km × 5 km) with *in situ* observations collected at a single point. Since the retrievals are based on look-up values and not the actual observed conditions, the complexity of the impacts of incorrect values might also contribute to these disparities.

Grid-based retrievals were attempted, but due to a lack of a dataset to validate the results, these have not been shown in this article.

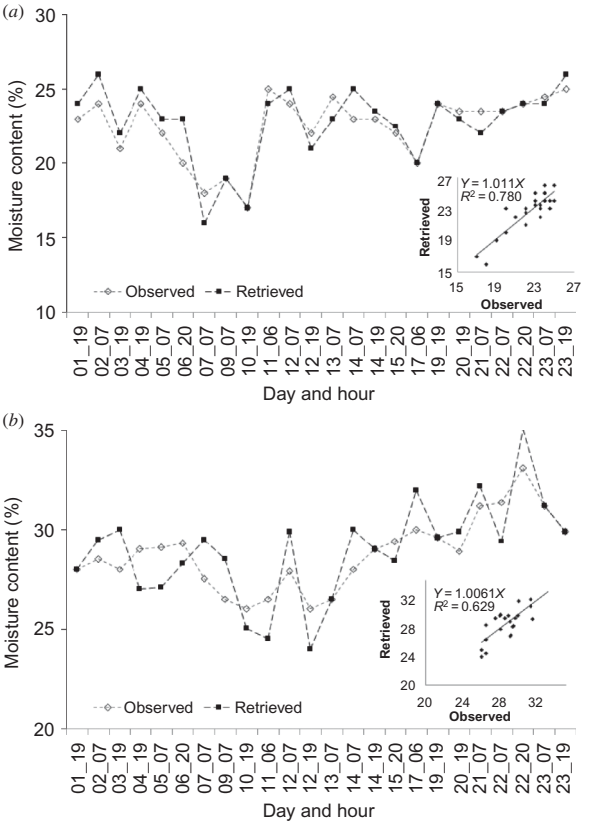


Figure 9. LUT retrieval results compared with observed soil moisture at two *in situ* stations for the month of August 2004: (*a*) BJ retrievals and (*b*) D110 retrievals. Insets show scatterplots of retrieved soil moisture against *in situ* soil moisture (%).

## 6. Conclusion

The objectives set out have been achieved. In this article, a fully coupled RTM (LA-RTM) that is capable of simulating observed brightness temperatures was developed and presented. This model is a coupling of various RTMs. LA-RTM is able to capture the radiative-transfer processes occurring over ocean surfaces fairly accurately. It was shown that LA-RTM is able to model satellite brightness temperatures over land and over ocean surfaces when the atmosphere state is reliably provided. From applications over Wakasa Bay, LA-RTM was shown as being able to nearly replicate observed brightness temperatures for both the AMSR-E and the GBMR cases.

In the case of Tibet, there were no GBMR observations and only AMSR-E data were used. From comparisons of LA-RTM simulated brightness temperatures and AMSR-E brightness temperatures, it was demonstrated that LA-RTM was able to capture the coupled effect of the atmosphere and land. It can thus be used to assist in studying atmosphere states over land at microwave frequencies.

As an offshoot of the research, it was shown that, given good initial conditions, the ARPS mesoscale model is able to generate atmosphere profiles that are in agreement

with sonde profiles. By using this mesoscale product, forecast information about the detailed atmosphere state can be obtained. These can be used in case atmosphere sounding data are missing, or are deemed to be inadequate and unreliable, such as in ungauged basins.

A retrieval scheme has been proposed that employs PI and ISW to retrieve surface-roughness conditions and near-surface soil moisture. These retrieved variables can be used to drive LA-RTM as a forward model to obtain corresponding emissivity or brightness temperatures at higher frequencies to assist in studying the impacts of atmosphere conditions over land. It was demonstrated that this retrieval scheme is capable of retrieving near-surface soil-moisture conditions reasonably well.

There are various areas that will be the target for subsequent research activities, such as the validity of the assumption that roughness conditions are time invariant. This may hold for a few days, but how long should the time frame for the invariance be? It is expected that some conditions may modify the roughness conditions, such as a precipitation event. The proposed strategy is to use a data-assimilation approach where all the observations and the forward model are ingested into an assimilation scheme and attempts made to arrive at better quantitative and qualitative results, especially with regard to spatial distribution of the roughness parameters and soil moisture, as was carried out in Yang *et al.* (2007).

While there is significant work that needs to be carried out, especially in the modelling of permafrost and mixed pixels (partly water and partly land) in the proposed model, it can nevertheless be applied in ungauged basins to improve understanding of the water and energy budgets in such basins. This can be realized by using time-series AMSR-E data to determine some of the temporally invariant parameters, which are then be fed back to determine the time-variant parameters and quantities in a scheme similar to that proposed by Yang *et al.* (2007). This proposed approach follows a two-step iterative procedure as follows:

Step 1 Utilize time-series satellite data, *in situ* observations and the retrieval scheme (or LA-RTM) and fix the time-invariant parameters. The time-invariant parameters are determined via sensitivity analysis.
Step 2 Using step 1 parameters and the same datasets and model, determine (retrieve) the time-varying variables.
Step 3 Feed step 2 results back to step 1 to refine invariant parameter estimation. This procedure can be repeated until there is convergence or when some specified number of iterations have been reached. *This step is optional.*

**Acknowledgements**

This study was carried out as part of the CEOP and Verification Experiment for AMSR/AMSR-E. Model-validation data were provided by the CEOP University of Tokyo Data Archiving Manager Mr. Katsunori Tamagawa. Sonde data were provided by Dr. Kenji Taniguchi. The authors would like to thank them for their support towards this research effort. The authors wish to acknowledge the critical input of the two peer reviewers who helped to improve the overall scholarly content of this work. This research was supported in part by the Japanese Science and Technology corporation for promoting Science and Technology in Japan, and in part by the Japan Aerospace Exploration Agency.

## References


Dobson, M.C., Ulaby, F.T., Hallikainen, M.T. and El-Rayes, M.A., 1985, Microwave dielectric behavior of wet soil – part II: dielectric mixing models. *IEEE Transactions on Geoscience and Remote Sensing*, **23**, pp. 35–46.

Fujii, H. and Koike, T., 2001, Development of a TRMM/TMI algorithm for precipitation in the Tibetan Plateau by considering effects of land surface emissivity. *Journal of the Meteorological Society of Japan*, **79**, pp. 475–483.

Jackson, T.J. and Schmugge, T.J., 1991, Vegetation effects on the microwave emission of soils. *Remote Sensing of Environment*, **36**, pp. 203–212.

Koike, T., Tsukamoto, T., Kumakura, T. and Lu, M., 1996, Spatial and seasonal distribution of surface wetness derived from satellite data. In *Proceedings of the International Workshop on Macro-scale Hydrological Modeling,* X. Liu and J. Li (Eds.), pp. 87–96, (Nanjing, China: Hohai University Press).

Kummerow, C., Hong, Y., Olson, W.S., Yang, S., Adler, R.F., McCollum, J., Ferraro, R., Petty, G., Shin, D. and Wilheit, T.T., 2001, The evolution of the Goddard Profiling Algorithm (GPROF) for rainfall estimation from passive microwave sensors. *Journal of Applied Meteorology*, **40**, pp. 1801–1820.

Kuria, D., Koike, T., Lu, H., Tsutsui, H. and Graf, T., 2007, Field-supported verification and improvement of a passive microwave surface emission model for rough, bare and wet soil surfaces by incorporating shadowing effects. *IEEE Transactions on Geoscience and Remote Sensing*, **45**, pp. 1207–1216.

Liu, G., 1998, A fast and accurate model for microwave radiance calculations. *Journal of the Meteorological Society of Japan*, **76**, pp. 335–343.

Lu, H., 2006, Development of a microwave radiative transfer model for a soil layer and its application to satellite remote sensing of soil moisture. PhD thesis, University of Tokyo, Japan.

Marshall, J.S. and Palmer, W.M., 1948, The distribution of raindrops with size. *Journal of Meteorology*, **5**, pp. 165–166.

Nemoto, T., Koike, T. and Kitsuregawa, M., 2007, Data analysis system attached to the CEOP centralized data archive system. *Journal of the Meteorological Society of Japan*, **85A**, pp. 529–543.

Njoku, E.G., 1999, *AMSR Land Surface Parameters. Algorithm Theoretical Basis Document, Version 3.0.* (Pasadena, CA: NASA Jet Propulsion Laboratory).

Paloscia, S. and Pampaloni, P., 1988, Microwave polarization index for monitoring vegetation growth. *IEEE Transactions on Geoscience and Remote Sensing*, **26**, pp. 617–621.

Peplinski, N.R., Ulaby, F.T. and Dobson, M.C., 1995, Dielectric properties of soil in the 0.3–1.3 GHz range. *IEEE Transactions on Geoscience and Remote Sensing*, **33**, pp. 803–807.

Pfaff, T., 2003, Remote sensing of snowfall and cloud liquid water using ground based passive microwave radiometry. Master's thesis, University of Tokyo, Japan.

Rose, R. and Zimmermann, R., 2003, RPG 2 channel radiometers and profilers. Radiometer physics GbmH. Available online at: www.radiometer-physics.de/rpg/html/docs/Manual_Profilers.pdf (last accessed 2 December 2010).

Schmugge, T.J. and Jackson, T.J., 1992, A dielectric model of the vegetation effects on the microwave emission from soils. *IEEE Transactions on Geoscience and Remote Sensing*, **30**, pp. 757–760.

Sekhon, R. and Srivastava, R., 1970, Snow size spectra and radar reflectivity. *Journal of the Atmospheric Sciences*, **27**, pp. 299–307.

Sellers, P.J., Los, S.O., Tucker, C.J., Justice, C.O., Dazlich, D.A., Collatz, G.J. and Randall, D.A., 1996, A revised land surface parameterization (SiB2) for atmospheric GCMs: part II – the generation of global fields of terrestrial biophysical parameters from satellite data. *Journal of Climate*, **9**, pp. 706–737.

Shin, D. and Kummerow, C., 2003, Parametric rainfall retrieval algorithms for passive microwave radiometers. *Journal of Applied Meteorology*, **42**, pp. 1480–1496.

Ulaby, F.T., Moore, R.K. and Fung, A.K., 1981, *Microwave Remote Sensing: Fundamentals and Radiometry*, vol. 1 (Norwood, MA: Artech House).

Ulaby, F.T., Moore, R.K. and Fung, A.K., 1986, Microwave backscatter dependence on surface roughness, soil moisture and soil texture for bare soil. *IEEE Transactions on Geoscience and Remote Sensing*, **16**, pp. 286–295.

West, R., Tsang, L. and Winebrenner, D.P., 1993, Dense medium radiative transfer theory for two scattering layers with a Rayleigh distribution of particles sizes. *IEEE Transactions on Geoscience and Remote Sensing*, **31**, pp. 426–437.

Wilheit, T., Kummerow, C. and Ferraro, R., 1999, *EOS/AMSR Rainfall. Algorithm Theoretical Basis Document* (Pasadena, CA: NASA Jet Propulsion Laboratory).

Xue, M., Wang, D., Gao, J., Brewster, K. and Droegemeier, K.K., 2003, The Advanced Regional Prediction System (ARPS), storm-scale numerical weather prediction and data assimilation. *Meteorology and Atmospheric Physics*, **82**, pp. 139–170.

Yang, K., Koike, T., Ye, B. and Bastidas, L., 2005, Inverse analysis of the role of soil vertical heterogeneity in controlling surface soil state and energy partition. *Journal of Geophysical Research*, **110**, D08101, doi:10.1029/2004JD005500.

Yang, K., Watanabe, T., Koike, T., Li, X., Fujii, H., Tamagawa, K., Ma, Y. and Ishikawa, H., 2007, Auto-calibration system developed to assimilate AMSR-E data into a land surface model for estimating soil moisture and the surface energy budget. *Journal of the Meteorological Society of Japan*, **85A**, pp. 229–242.

Yang, K., Chen, Y.Y. and Qin, J., 2009, Some practical notes on the land surface modeling in the Tibetan Plateau. *Hydrology and Earth System Sciences Discussions*, **6**, pp. 1291–1320.